Equilibrium Dynamics of Mutually Confined Waves with Signed Analogous Masses

Ping Zhang, Qing Guo, Hao Wu, Zeyu Gong, Binbin Nie, Yi Hu,[*] Zhigang Chen, and Jingjun Xu[†]

The MOE Key Laboratory of Weak-Light Nonlinear Photonics, TEDA Applied Physics Institute and
School of Physics, Nankai University, Tianjin 300457, China

We report the first experimental realization of equilibrium dynamics of mutually confined waves with signed analogous masses in an optical fiber. Our Letter is mainly demonstrated by considering a mutual confinement between a soliton pair and a dispersive wave experiencing opposite dispersion. The resulting wave-packet complex is found robust upon random perturbation and collision with other waves. The equilibrium dynamics are also extended to scenarios of more than three waves. Our finding may trigger fundamental interest in the dynamics of many-body systems arising from the concept of negative mass, which is promising for new applications based on localized nonlinear waves.

Negative mass generally introduces counterintuitive effects. Typically, a negative-mass object tends to move against an applied force, in sharp contrast to the experience commonly encountered in our everyday lives. Analogous phenomena also exist for waves, as represented by the well-known example: the electrons at the top and bottom edges of an energy band move in opposite directions upon an identical static electric field. Basically, such different wave dynamics stem from the inverted wave spreading (characterized by dispersion relation in general), which has been proven ubiquitous in nature [1–3]. Negative-mass dynamics have been realized via dispersion management in different branches of physics such as in optics, cold atoms, and acoustics, and interestingly, its realization was extended to the nonlinear regime [4,5].

The exotic feature of negative-mass matter is well-manifested in its interaction with positive-mass matter [6], inspiring the ideas of propellant-free propulsion [7], explaining dark matter and energy [8], and even constructing static vacuum black holes [9]. Given that negative-mass matter is still inaccessible, nonlinear optics offers a convenient and feasible platform to study this intriguing phenomenon in an analogous way. For example, the so-called runaway motion, a kind of self-propulsion solely driven by the interaction of matters with opposite mass signs, was demonstrated initially in nonlinear fiber optics [10,11] and later extended to the optical spatial domain [12,13], leading to a wealth of advanced light manipulation technology. Recently, this diametric drive behavior attracted attention from the field of Bose-Einstein condensates [14], and was shown to exhibit unique wave features [15] in connection to another widely explored self-accelerating effect associated with Airy wave packets [16–19]. During such a synchronized motion, two involved waves bind together to form a wave complex, which is fundamentally different from soliton bound states [20–30].

The resulting binding has to be accompanied with a self-accelerating effect, leading to the fact that the temporal localization must coexist with a frequency shift. To break this linkage, one may consider scenarios involving more waves. Indeed, the equilibrium dynamics of multiwaves with signed masses were earlier considered [31–33] for the purpose of realizing localized pulses in the normal dispersion regime of fibers and further being used to increase the capacity of optical communication [34]. But thus far, this interesting nonlinear interaction has not been observed in experiment to the best of our knowledge.

In this Letter, we demonstrate experimentally the first nonlinear binding and equilibrium dynamics of multiple interacting waves involving signed analogous masses in an optical fiber. The first example is an optical pulse complex consisting of a soliton pair and a dispersive wave that have opposite signs of analogous mass. The mutually confined entity shows a robust feature against strong random perturbation, or upon certain collisions with other optical pulses. Our method is also extended to cases involving more than three waves.

At first, we present the basic idea to form a pulse complex by using the three-wave configuration initially proposed in Refs. [31–33] and illustrated in Fig. 1. Considering two closely separated out-of-phase (π phase difference) solitons, subject to anomalous group-velocity dispersion (GVD), they repel each other upon nonlinear interaction (Fig. 1(a)) [35]. A dispersive wave alone, in the inverted dispersion regime (i.e., normal GVD), would experience a self-defocusing nonlinear evolution [Fig. 1(b)]. The three waves are able to bind together while reach an equilibrium state [Fig. 1(c)]: the dispersive wave is trapped by the soliton pair against the self-defocusing effect, and meanwhile the repulsion separating the two solitons is balanced by the attraction offered by the dispersive wave [36–39].
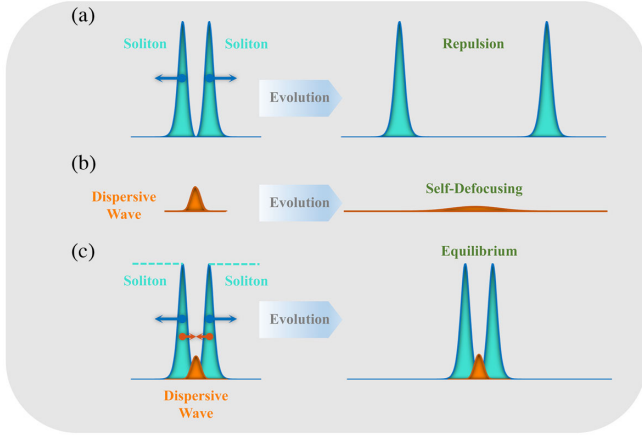
FIG. 1. Schematic diagram illustrating a nonlinear binding of three waves with signed masses in an optical analog. (a) Two out-of-phase solitons repel each other; (b) a dispersive wave undergoes a self-defocusing evolution; (c) the soliton pair and the dispersive wave reach an equilibrium state upon their mutual interaction.
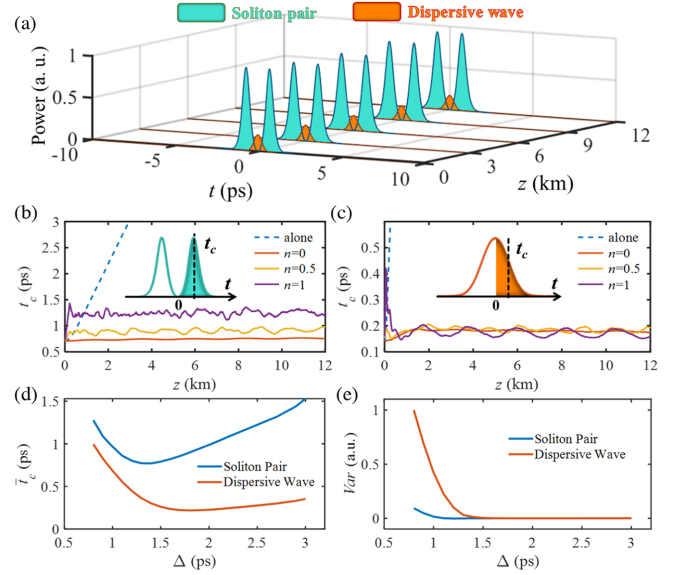

FIG. 2. Numerically calculated pulse complexes and their evolution. (a) Propagation of a typical pulse complex. (b),(c) Spreading (characterized by t_c: "center of mass" of a pulse at $t > 0$) of the soliton pair (b) and the dispersive wave (c) in (a): solid lines are associated with the scenarios where they mutually interact at different levels of random noise (whose strength is characterized by the parameter n defined in text) applied at the input, while dashed lines plot the case when either of them propagates alone. (d) The pulse spreading averaged along a 12-km-long distance for complexes designed with various soliton separations. (e) Variance analysis of the spreading (in terms of t_c) during propagation corresponding to the cases in (d).

To design the equilibrium state, we employ the coupled nonlinear Schrödinger equations that govern the pulse propagation and interactions in optical fibers [40]:

$$i\frac{\partial A}{\partial z} = \frac{\beta_{2A}}{2}\frac{\partial^2 A}{\partial t^2} - \gamma_A(|A|^2 + 2|B|^2)A, \quad (1a)$$

$$i\frac{\partial B}{\partial z} = \frac{\beta_{2B}}{2}\frac{\partial^2 B}{\partial t^2} - \gamma_B(2|A|^2 + |B|^2)B, \quad (1b)$$

where A and B present the pulse envelopes of a soliton pair and a dispersive wave, respectively, z is the propagation distance, t is time in the frame moving at a group velocity shared by all the three pulses, β_{2A} (β_{2B}) is the anomalous (normal) GVD coefficient, and the coefficients γ_A and γ_B indicate the nonlinear strength. In the following analysis, we adopt the fiber parameters used in our experimental setting: $\beta_{2A} = -1.3 \times 10^{-3}$ ps^2 m^{-1}, $\beta_{2B} = 1.2 \times 10^{-3}$ ps^2 m^{-1}, and $\gamma_A = \gamma_B = 0.5 \times 10^{-3}$ W^{-1} m^{-1}. The two out-of-phase solitons are expressed as $A(t,z=0) = \sqrt{P_A}\text{sech}[(t-\Delta/2)/T_A] - \sqrt{P_A}\text{sech}[(t+\Delta/2)/T_A]$, where P_A is the peak power, $T_A = [|\beta_{2A}|/(\gamma_A P_A)]^{1/2}$ characterizes the pulse duration of each soliton, and Δ introduces a temporal separation between them. Assuming that their repulsion is counteracted by the force exerted by the dispersive wave, the index changes induced nonlinearly by the solitons form a static potential well for the dispersive wave in the retarded frame. Consequently, Eq. 1(b) becomes a nonlinear eigenvalue problem as described by

$$\nu B = \frac{\beta_{2B}}{2}\frac{\partial^2 B}{\partial t^2} - \gamma_B(2|A|^2 + |B|^2)B, \quad (2)$$

where ν is the eigenvalue. To obtain a localized solution, the solitons are artificially flattened in the region outside the two peaks [Fig. 1(c)], thus avoiding the tunneling effect in this finite potential well. This approximation was proven valid for analyzing the two-body interactions [10,15]. Note that our design method is different from the ones employed in Refs. [31–34]. By choosing a proper value of ν, a desired dispersive wave used for balancing the soliton repulsion is obtained. Figure 2(a) presents an example of the achieved three-body system. Along the propagation, the soliton pair and the dispersive wave reach an equilibrium during their interaction. To quantify their spreading, the "center of mass" is analyzed using just half of each pulse profile (say, in the region of $t > 0$). It is expressed as $t_c = \int_0^\infty |\psi|^2 t dt / \int_0^\infty |\psi|^2 dt$ (where ψ refers to pulse A or B), which typically goes up when the pulse undergoes broadening. Because of the binding effect, the values of t_c for both the soliton pair and the dispersive wave are kept nearly constant during propagation [Figs. 2(b) and 2(c)]. In contrast, the "center of mass" t_c for either of them propagating alone increases dramatically, induced by the repulsion or the self-defocusing effect. Furthermore, the scenarios for different soliton spacings are considered. To this end, t_c is averaged along the propagation distance, i.e., $\bar{t}_c = \int_0^L t_c dz/L$ (where L is a fiber length). Its value in terms of the spacing Δ is presented in Fig. 2(d) for a fixed soliton peak power (i.e., $P_A = 30$ W). In general, as the two solitons are set closer, the

resulting pulse complex has a smaller duration. This does not hold for $\Delta \lesssim 1.3$ ps, where the solved dispersive wave manifests a considerable tunneling that is adverse to further reducing the temporal scale of the complex. Under these conditions, the generated pulse complex undergoes an apparently breathing dynamic, as shown by the variances of t_c [Fig. 2(e)]. The breathing effect is more obvious for the dispersive wave. Indeed, due to the existence of the tunneling effect, such a three-body interaction is always in a quasie-quilibrated regime. But for a large soliton spacing, the pulse jitters induced by the breathing effect are negligible when compared with the duration of the associated pulse complex [Fig. 2(e)].

We also examine the robustness of this kind of three-body system by imposing a random noise as the perturbation to the involved pulses at the input. The noises added on the soliton pair and the dispersive wave are expressed as $nf(t)A(t)$ and $nf'(t)B(t)$, respectively, where $f(t)$ and $f'(t)$ includes random values with a uniform distribution between -0.5 and 0.5, and n defines the noise strength. As a typical example, the pulse complex presented in Fig. 2(a) are used for the test. The applied noise causes a pulse spreading at the onset of the propagation for both the soliton pair and the dispersive wave [Figs. 2(b) and 2(c)]. This change comes earlier and becomes larger upon a stronger noise. But eventually, the spreading ceases, followed by a weak oscillation of the pulse duration (characterized by t_c). In principle, this stability originates from the robustness of solitons that can bear a strong perturbation.

Next, we carry out experiments using the setup schematically plotted in Fig. 3(a) to demonstrate the binding effect. The soliton pair and the dispersive wave are generated by reshaping a femtosecond pulse featuring a broadband spectrum and then properly amplified by an erbium-doped fiber amplifier. This process involves a programmable pulse shaper that encodes the spectral information of the prede-signed pulse complex (see Supplemental Material [41]). The nonlinear pulse propagation takes place in a dispersion-shifted fiber (4 km long) with a zero-dispersion wavelength at 1547.7 nm. The soliton pair and the dispersive wave, whose center wavelengths are selected to be 1561 nm and 1536 nm, respectively, experience the same group velocity but opposite GVDs. The input and output pulses are measured both in temporal and spectral domains via a frequency-resolved optical gating system and an optical spectrum analyzer, respectively.

In order to avoid the influence of the intrapulse Raman effect [42] that generally induces a soliton deceleration (accordingly a frequency shift), the two solitons are designed to feature a large duration. Figure 3(b) presents the input and output profiles of a pulse complex. As expected, the soliton pair and the dispersive wave remain bound in subsequent nonlinear evolution. A small spreading is observed for the pulse complex at the output, which is caused by the fact that the theoretical model shown in
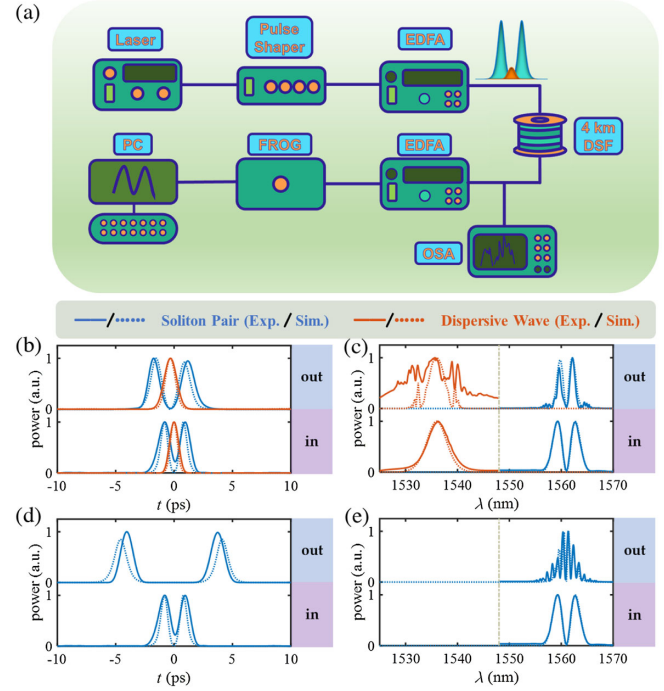

FIG. 3. Experimental demonstration of a nonlinear binding of three waves in an optical fiber. (a) Schematic setup; (b) temporal and (c) spectral profiles of the pulse complex consisting of a soliton pair and a dispersive wave at the input (bottom panels) and output (upper panels). (d),(e) Temporal and spectral profiles corresponding to (b),(c) but for the case that the soliton pair propagates alone. (FROG, frequency-resolved optical gating; EDFA, ermium-doped fiber amplifier; OSA, optical spectrum analyzer).

Eq. (1) does not fully describe the realistic propagation environment. For reproducing our experimental results, we perform numerical simulations by also involving the loss and third-order dispersion existing in the fiber, character-ized by α and β_3, respectively. In this framework, Eqs. (1a) and (1b) are modified as

$$i\frac{\partial A}{\partial z} = \frac{\beta_{2A}}{2}\frac{\partial^2 A}{\partial t^2} + i\frac{\beta_3}{6}\frac{\partial^3 A}{\partial t^3} - \gamma_A(|A|^2 + 2|B|^2)A - \frac{i\alpha}{2}A,$$

$$i\frac{\partial B}{\partial z} = \frac{\beta_{2B}}{2}\frac{\partial^2 B}{\partial t^2} + i\frac{\beta_3}{6}\frac{\partial^3 B}{\partial t^3} - \gamma_B(|B|^2 + 2|A|^2)B - \frac{i\alpha}{2}B \ .$$

$$(3)$$

Here, the dispersion terms of orders higher than third-order dispersion and higher-order nonlinear effects are safely neglected as the input pulses have a large duration (~ 1 ps). By adopting the fiber parameters $\beta_3 = 1 \times 10^{-4}$ ps^3 m^{-1} and $\alpha = 0.33$ dB/km, the experimental observations are well-reproduced in simulations. Good agreement is also reached in the spectral domain [Fig. 3(c)]. As a result of this binding effect, the spectral feature is almost maintained from the input to the output. The center wavelengths for both the soliton pair and the dispersive wave remain

unchanged, validating the omittance of the Raman effect in our simulations. Note that the pedestal in the measured spectrum of the dispersive wave comes from the pump source of the erbium-doped fiber amplifier, which almost has null influence on the nonlinear interaction. Detailed simulations show that the weakened confinement at the output is mainly caused by the loss, while the sidebands observed in the spectra of the soliton pair and the dispersive wave are mainly associated with cross-phase modulation and four-wave mixing, respectively. As a reference, the two solitons are also injected into the dispersion-shifted fiber without the dispersive wave in experiment. They separate far away at the output upon their repulsion [Fig. 3(d)]. Accordingly, their spectrum exhibits fringes [Fig. 3(e)], losing the input feature of two peaks. This direct comparison experiment and its agreement with the numerical simulation further confirm the formation of the pulse complex observed in Figs. 3(b) and 3(c). Our additional simulations show that the nonlinear binding tends to be weakened under the action of higher order nonlinearities, but the timescale of the three pulses is still much smaller than the temporal separation of the two solitons propagating alone (see Supplemental Material [41]). These perturbation effects, including higher order nonlinearities and dispersions, can be largely mitigated by designing pulse complexes featured with a long duration [40] (see also Supplemental Material [41]), or by properly choosing fibers where these effects are small [33].

We further test the robustness of this nonlinear binding upon collision with other waves. For this purpose, another pulse in the normal GVD regime is introduced to collide with the pulse complex. This external pulse is imparted a Gaussian shape expressed as $\sqrt{\zeta P_B}\exp[-(t-\delta)^2/w^2]\exp(-i\rho t)$, where ζ, δ, w, and ρ characterize its intensity (in terms of the peak power of the dispersive wave, i.e., P_B), delay, duration, and initial kick, respectively. In simulations, different values of ζ are employed, while the other parameters are fixed at $\delta=2.5$ ps, $w=0.5$ ps, and $\rho=1$ THz. Numerical outputs for various input conditions are shown in Fig. 4(a). Clearly, the pulse complex preserves when the impinging pulse is not too intense. As the intensity of the external pulse turns up too high, the pairing solitons become unequal in intensity. When $\zeta > 2$, the soliton pair is totally destroyed and thus fails to confine a dispersive wave between them. Two typical examples that visualize the pulse propagation are presented in Figs. 4(b)–(e) to illustrate the stable and unstable regimes. In the case of the weak external pulse ($\zeta=1$), all the components in the pulse complex experience an oscillatory evolution after the collision. The dispersive wave shows a time jitter, while the soliton pair becomes asymmetric with the peak power alternatively switching between its two components. However, they can still bind together, showing a stable feature [Figs. 4(b) and 4(d)]. When the external pulse is too strong ($\zeta=3.5$), the same pulse complex can only sustain for a limited distance [Figs. 4(c) and 4(e)]. After that, it exhibits a dramatic distortion: the energy of the trailing
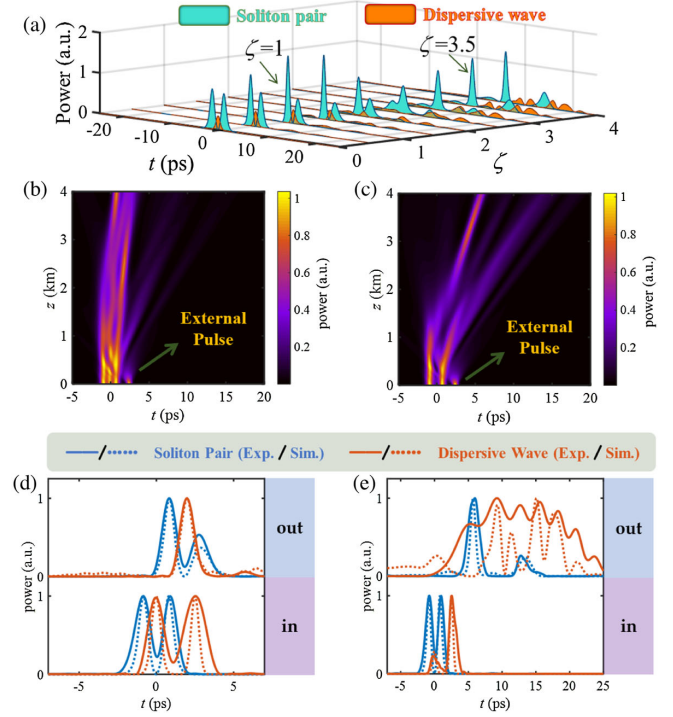

FIG. 4. Evolution of a pulse complex upon colliding with an external pulse. (a) Output profiles of the complex impinged by the external pulse having various input intensities; (b)–(e) numerical propagation (b),(c) and input/output profiles (d),(e) for the cases of $\zeta=1$ (b),(d) and 3.5 (c),(e). Experimentally measured input/output profiles are also plotted in (d),(e) in solid curves.

soliton is largely transferred to the leading one, thus losing the pair structure to trap the dispersive wave that eventually mixes with the external pulse to form a fringe pattern. In experiment, similar features are observed at the output by using the input conditions close to the numerical simulations [Figs. 4(d) and 4(e)]. Additional simulated scenarios, presenting the interactions between two pulse complexes, also show the ability of this mutually confined state to sustain certain collisions (see Supplemental Material [41]).

Our design method can be readily extended to form pulse complexes involving more solitons and dispersive waves [see Figs. 5(a) and 5(b) and Supplemental Material [41]]. In experiment, we realize the case of three solitons [Fig. 5(c)]. As a result of the nonlinear binding, the three solitons copropagating with the associated dispersive waves show a smaller separation comparing to the case where they propagate alone (more experimental data are presented in Supplemental Material [41]). Note that it is a challenge to observe pulse complexes for further increasing the number of solitons due to the resolution limit of the state-of-the-art pulse shaper.

In conclusion, we have experimentally demonstrated equilibrium dynamics of mutually confined waves with signed analogous masses in an optical fiber. We realize a cross-trapping between a soliton pair and a dispersive wave. The resulting pulse complex is stable against random
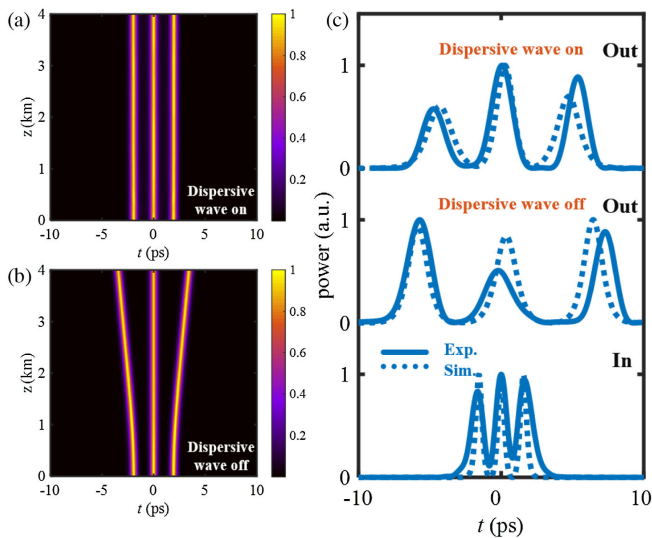
FIG. 5.   Three solitons used to realize an equilibrium state with the assistance of dispersive waves (not shown here). (a),(b) Numerical propagation of the solitons in the presence (a) and absence (b) of the dispersive waves (Note: third-order dispersion and loss are not considered). (c) Measured solitons at the input (bottom panel) and their output profiles for the case that the desired dispersive waves are switched on (upper panel) or off (middle panel). In (c), the simulations are obtained by using the realistic model [i.e., Eq. (3)].

noise and can preserve their structures during certain collisions with other pulses. Furthermore, we extend the equilibrium dynamics to multiwave interactions by including more solitons. Our Letter could trigger fundamental interests in investigating many-body interactions involving the concept of negative mass. From the application viewpoint, the results may spark new ideas for realizing pulse complexes beneficial to increasing the transmission capacity in fiber communications [23].

P. Z. and Q. G. contributed equally to this work.

---

[*]yihu@nankai.edu.cn
[†]jjxu@nankai.edu.cn

[1] Z. Liu, X. Zhang, Y. Mao, Y. Y. Zhu, Z. Yang, C. T. Chan, and P. Sheng, Science **289**, 1734 (2000).
[2] C. Luo, S. G. Johnson, J. D. Joannopoulos, and J. B. Pendry, Phys. Rev. B **65**, 201104(R) (2002).
[3] O. Morsch and M. Oberthaler, Rev. Mod. Phys. **78**, 179 (2006).
[4] F. Di Mei, P. Caramazza, D. Pierangeli, G. Di Domenico, H. Ilan, A. J. Agranat, P. Di Porto, and E. DelRe, Phys. Rev. Lett. **116**, 153902 (2016).
[5] L.-C. Zhao, W. Wang, Q. Tang, Z.-Y. Yang, W.-L. Yang, and J. Liu, Phys. Rev. A **101**, 043621 (2020).
[6] H. Bondi, Rev. Mod. Phys. **29**, 423 (1957).
[7] M. G. Millis, J. Propul. Power **13**, 577 (1997).
[8] J. S. Farnes, Astron. Astrophys. **620**, A92 (2018).
[9] M. Khuri, G. Weinstein, and S. Yamada, Phys. Rev. D **104**, 044063 (2021).
[10] S. Batz and U. Peschel, Phys. Rev. Lett. **110**, 193901 (2013).
[11] M. Wimmer, A. Regensburger, C. Bersch, M.-A. Miri, S. Batz, G. Onishchukov, D. N. Christodoulides, and U. Peschel, Nat. Phys. **9**, 780 (2013).
[12] Y. Pei, Y. Hu, C. Lou, D. Song, L. Tang, J. Xu, and Z. Chen, Opt. Lett. **43**, 118 (2018).
[13] Y. Pei, Y. Hu, P. Zhang, C. Zhang, C. Lou, C. E. Rüter, D. Kip, D. Christodoulides, Z. Chen, and J. Xu, Opt. Lett. **44**, 5949 (2019).
[14] H. Sakaguchi and B. A. Malomed, Phys. Rev. E **99**, 022216 (2019).
[15] P. Zhang, Y. Hu, D. Bongiovanni, Z. Li, R. Morandotti, Z. Chen, and J. Xu, Phys. Rev. Lett. **127**, 083901 (2021).
[16] M. V. Berry and N. L. Balazs, Am. J. Phys. **47**, 264 (1979).
[17] G. A. Siviloglou, J. Broky, A. Dogariu, and D. N. Christodoulides, Phys. Rev. Lett. **99**, 213901 (2007).
[18] G. A. Siviloglou and D. N. Christodoulides, Opt. Lett. **32**, 979 (2007).
[19] N. K. Efremidis, Z. Chen, M. Segev, and D. N. Christodoulides, Optica **6**, 686 (2019).
[20] N. N. Akhmediev, A. Ankiewicz, and J. M. Soto-Crespo, Phys. Rev. Lett. **79**, 4047 (1997).
[21] M. Mitchell, M. Segev, and D. N. Christodoulides, Phys. Rev. Lett. **80**, 4657 (1998).
[22] E. A. Ostrovskaya, Y. S. Kivshar, D. V. Skryabin, and W. J. Firth, Phys. Rev. Lett. **83**, 296 (1999).
[23] M. Stratmann, T. Pagel, and F. Mitschke, Phys. Rev. Lett. **95**, 143902 (2005).
[24] F. Amrani, A. Niang, M. Salhi, A. Komarov, H. Leblond, and F. Sanchez, Opt. Lett. **36**, 4239 (2011).
[25] D. C. Cole, E. S. Lamb, P. Del'Haye, S. A. Diddams, and S. B. Papp, Nat. Photonics **11**, 671 (2017).
[26] O. Melchert, S. Willms, S. Bose, A. Yulin, B. Roth, F. Mitschke, U. Morgner, I. Babushkin, and A. Demircan, Phys. Rev. Lett. **123**, 243905 (2019).
[27] W. Weng, R. Bouchand, E. Lucas, E. Obrzud, T. Herr, and T. J. Kippenberg, Nat. Commun. **11**, 1 (2020).
[28] F. Kurtz, C. Ropers, and G. Herink, Nat. Photonics **14**, 9 (2020).
[29] W. He, M. Pang, D.-H. Yeh, J. Huang, P. Russell, and J. St, Light Sci. Appl. **10**, 1 (2021).
[30] O. Melchert, S. Willms, I. Babushkin, U. Morgner, and A. Demircan, Optik (Stuttgart) **280**, 170772 (2023).
[31] D. Anderson, A. Hook, M. Lisak, V. N. Serkin, and V. V. Afanasjev, Electron. Lett. **28**, 1797 (1992).
[32] A. Hook, D. Anderson, M. Lisak, V. N. Serkin, and V. V. Afanasjev, J. Opt. Soc. Am. B **10**, 2313 (1993).
[33] A. Hook and V. N. Serkin, IEEE J. Quantum Electron. **30**, 1 (1994).
[34] J. I. Da Silva and A. S. B. Sombra, Opt. Commun. **152**, 59 (1998).
[35] F. M. Mitschke and L. F. Mollenauer, Opt. Lett. **12**, 355 (1987).

[36] A. V. Gorbach and D. V. Skryabin, Nat. Photonics **1**, 653 (2007).

[37] T. G. Philbin, C. Kuklewicz, S. Robertson, S. Hill, F. Konig, and U. Leonhardt, Science **319**, 1367 (2008).

[38] A. Demircan, S. Amiranashvili, and G. Steinmeyer, Phys. Rev. Lett. **106**, 163901 (2011).

[39] S. F. Wang, A. Mussot, M. Conforti, X. L. Zeng, and A. Kudlinski, Opt. Lett. **40**, 3320 (2015).

[40] G. P. Agrawal, *Nonlinear Fiber Optics* (Springer, New York, 2000).

[41] See Supplemental Material at http://link.aps.org/supplemental/10.1103/PhysRevLett.131.087201 for additional numerical and experimental results for pulse complexes.

[42] F. M. Mitschke and L. F. Mollenauer, Opt. Lett. **11**, 659 (1986).